Chem. Pap. (2018) 72:235–250
https://doi.org/10.1007/s11696-017-0276-7

ORIGINAL PAPER

A novel catalyst of MIL-101(Fe) doped with Co and Cu as persulfate activator: synthesis, characterization, and catalytic performance

Mei-Juan Duan[1] · Ze-yu Guan[4] · Yong-Wen Ma[1,2,3] · Jin-Quan Wan[1,2,3] · Yan Wang[1,2,3] · Yan-Fei Qu[1]

Received: 8 March 2017 / Accepted: 16 August 2017 / Published online: 30 August 2017

Abstract In this work, effective and novel heterogeneous catalysts of Metal–organic framework MIL-101(Fe) doped with cobalt (Co^{2+}) or copper (Cu^{2+}) have been synthesized by post-synthesis method, namely Co–MIL-101(Fe) and Cu–MIL-101(Fe). The initial and metal-doped samples were tested to activate persulfate (PS) for removal of Acid Orange 7 (AO7) in water. The surface of samples were characterized using X-ray diffraction, Fourier transform infrared spectroscopy, Raman spectroscopy, N_2 adsorption, scanning electron microscopy and transmission electron microscopy. The addition of Cu^{2+} and Co^{2+} could alter structure characteristics of MIL-101(Fe) in crystal structure and morphology. The unusual octahedron morphology of MIL-101(Fe) turned to be irregular, disorder and a rod-like morphology was shaped. What is more, Co doping caused greater changes in structure characteristics in comparison with Cu doping. The alteration was reflected in the catalytic capacity of PS activation. An interesting note was that, whether Co or Cu doping, metal-doped MIL-101(Fe) greatly improved the PS activation as compared to unmodified MIL-101(Fe). The removal rate of AO7 was about 66, 92, 98% in MIL-101(Fe)/PS, 6%wtCu–MIL-101(Fe)/PS and 6%wtCo–MIL-101(Fe)/PS system, respectively. Some results also suggested the performance of Co–MIL-101(Fe) was superior to that of Cu–MIL-101(Fe). Additionally, a series of parameters were designed to achieve maximum capacity of PS activation. Such an enhancement in activity may be attributed to the main reasons: the new active sites created by metal additives; an increase in number of active Fe sites produced by Co and Cu doping which results in alteration of morphology and structure of catalysts.

Keywords Metal–organic frameworks · Heterogeneous catalyst · Persulfate activation · Active iron sites

Introduction

Considerable attention has been paid to advanced oxidation processes (AOPs) due to its high efficiency for destruction of refractory contaminants, as shown by a series of researches (Klavarioti et al. 2009; Vallejo et al. 2015; Kurniawan et al. 2006). It has been demonstrated that the application of AOPs based on activation of persulfate anion ($S_2O_8^{2-}$, PS) to generate a strong oxidant, sulfate free radical ($SO_4^{\cdot-}$, $E^0 = 2.5–3.1$ V), displayed a great oxidation ability of dealing with contaminants (Waldemer et al. 2007; Fang et al. 2013). In previous work, heat, UV light, and transition metal ions (Me^{n+}) can excite PS to form sulfate radical to degrade organic pollutants (Nie et al. 2014; Lin et al. 2011; Oh et al. 2009). Compared with heat and UV light, transition metal activation has drawn much more attention due to its lower energy consumption, especially in heterogeneous activation of metal-based materials. Until now, most of the studies have been

✉ Ze-yu Guan
guanzeyu1@126.com

[1] School of Environment and Energy, South China University of Technology, Guangzhou 510006, China

[2] State Key Laboratory of Pulp and Paper Engineering, South China University of Technology, Guangzhou 510006, China

[3] The Key Laboratory of Pollution Control and Ecosystem Restoration in Industry Clusters, Ministry of Education, South China University of Technology, Guangzhou 510006, China

[4] School of Chemistry and Chemical Engineering, South China University of Technology, Guangzhou 510006, China

published on metal oxides and metal-doped materials to activate persulfate (PS) or peroxymonosulfate (PMS) for dealing with water pollutants (Pu et al. 2015; Li et al. 2014; Oh et al. 2010; Liang et al. 2013; Lin et al. 2017). However, with an aim to enhance the efficiency of heterogeneous metal-activated performance, some researchers integrated two or more metallic materials into PS activation system to exploit their synergistic effect (Lei et al. 2015; Sun et al. 2015).

Metal–organic frameworks (MOFs), referred as an extensive class of multifunctional inorganic–organic hybrid porous crystalline materials, where metal ions or clusters are linked to organic linkers (Zhou et al. 2012), have gained substantial interest with their unique feature of large pore size, high apparent surface areas and homogeneous active metal nodes. These characteristics allowed the interior of MOFs to be widely used in gas separation, drug delivery, and adsorption of targeted pollutants (Rocca et al. 2011; Li et al. 2009). In particular, due to their active metal sites, MOFs were widely used in the field of heterogeneous catalysis (Hwang et al. 2008; Fei et al. 2014). However, the coordination sphere of the metal ions in MOFs was fully linked or blocked by the organic linkers, then there were no free unsaturated metal nodes available to activate with some reactants, which could limit the possibilities of MOFs for the application in catalysis (Alaerts et al. 2006). For dealing with this drawback, a useful approach was proposed to prepare more active metal sites by introducing metal compounds to link with organic linkers of MOFs (Wu et al. 2013). Currently, as the water pollution getting been heavier, MOFs have also exhibited tremendous potential as effective activators in AOPs owing to their unsaturated metal nodes. Since the first report on photocatalytic activity in MOF-5 (Llabrés et al. 2007), an increasing number of MOFs have been found utility as photocatalyst (Shen et al. 2013; Zhang et al. 2015). Meanwhile, some MOFs or modified MOFs also been taken as heterogeneous catalyst of hydrogen peroxide (H_2O_2) to produce hydroxyl radicals ($OH^{\cdot}$) for the degradation of organic contaminants with the help of UV light [Zhao et al. 2015; Liang et al. 2015; Ai et al. 2014; Nguyen and Nguyen 2014). It is very common to find that iron-based MIL (MIL stands for Material of Institute Lavoisier)] not only possesses active sites (Fe^{III}) for heterogeneous Fenton reaction but also have the advantages of iron complex with homogeneous Fenton reaction due to its unique properties of organometallic coordination. That is to say, MIL samples can be potentially regarded as Fenton catalysts for removing organic contaminants. As H_2O_2 and PS are similar instructure of having O–O bond, naturally, we assume that PS also can be activated by MOFs. Lin et al. (2015) illustrated an iron-based metal organic framework, MIL-88A, which excited PS for the decomposition of Rhodamine B in water. However, for the purpose of enhancing decolorization of Rhodamine B, the author introduced heat to MIL-88A, which produced a better effectiveness than free-heat activation. Obviously, those MOFs showed their catalytic activity lie in the existence of the unsaturated metal sites.

Iron, which has been demonstrated to effectively degrade most of the contaminants via persulfate activation. Herein, considering that iron metal is an environmentally benign, abundant and cheap component with non-toxicity, we choose MIL-101(Fe), an iron-based MOF built up from octahedral chains of Fe^{III} and 1,4-benzenedicarboxylic acid (H_2BDC), as heterogeneous catalyst of persulfate. MIL-101(Fe) features excellent porosity, high surface areas and large amounts of iron (Taylor-Pashow et al. 2009). However, the inherent lack of unsaturated metal sites may lead a dissatisfactory performance for contaminant degradation. For instance, Lv et al. (2015) designed Fe^{III}-doped MIL-100 with new active sites, Which can activate persulfate with high efficiency to decompose azo-dye. Thereby, it is feasible that incorporating other transition metals with MIL-101(Fe) to reinforce unsaturated metal sites for persulfate activation. Besides, other transition metals such as copper (Cu^{II}) and cobalt (Co^{II}) also showed better performance of persulfate activation (Liang et al. 2013; Gayathri et al. 2009). Therefore, in this work, we report, for the first time, we illustrated the synthesis of Co^{II} or Cu^{II} supported MIL-101(Fe) [namely Cu–MIL-101(Fe), Co–MIL-101(Fe)] and their application for Acid Orange 7 (AO7) degradation via persulfate activation. In the light of composition of catalysts, a potential mechanism of persulfate activation by Cu–MIL-101(Fe) and Co–MIL-101(Fe) were also proposed and demonstrated.

Experimental

Materials and methods

Chemicals

All chemicals used in this work were analytical grade and without further purification. The water used in all the experiment was produced by a Millipore milli-Qsystem. Citric acid ($C_6H_8O_7{\cdot}H_2O$), Iron chloride hexahydrate ($FeCl_3{\cdot}6H_2O$), Copper(II) nitrate hydrate ($Cu(NO_3)_2{\cdot}3H_2O$) and Cobalt(II) nitrate hexahydrate ($Co(NO_3)_2{\cdot}6H_2O$) were purchased from Shanghai Future Chemical Technology Co., Ltd (Shanghai, China). Potassium persulfate, ethanol and *N*-dimethylformamide (DMF) were purchased from Tianjin Kemiou chemical Reagent Co., Ltd (Tianjin, China). And H_2BDC was provided by Aladdin Industrial Corporation (Shanghai, China). The

commercially available AO7 (purity > 99.0%) was supplied by Tokyo Chemical Industry (Japan).

Synthesis of Cu–MIL-101(Fe) and Co–MIL-101(Fe)

MIL-101(Fe) was synthesized according to the method developed by Skobelev et al. (2013) with a certain modification in purification. In brief, 0.675 g of $FeCl_3 \cdot 6H_2O$ and 0.206 g of H_2BDC were added to 25 mL DMF and the resulting mixture was stirred to fully dissolved. Subsequently, the homogeneous solution in a Teflon autoclave reactor of 100 mL was heated at 383 K for 24 h. The product was first collected via centrifugation. To thoroughly remove the DMF and excess H_2BDC, the product was purified by washing in hot ethanol (60 °C, 3 h, 2 times) and hot water (60 °C, 1 h, 1 time). Moreover, the collector was dried in a vacuum oven (150 °C, 12 h).

Co–MIL-101(Fe) was prepared by post-synthesis method. The idea of impregnation method came from an article described by Qin et al. (2015), which clearly indicated the adding of citric acid could allow more metal ions to be homogeneously plugged into the channels of MOFs. Therefore, the preparation of Co–MIL-101(Fe) can be illustrated as follows. First, 0.2 g of MIL-101(Fe) was added into an aqueous solution mixing cobalt nitrate and citric acid with a desired concentration, the slurry was stirred for 4 h to form homogeneous mixture and then heated in a Teflon autoclave reactor at 353 K for 8 h. After that, the collected powder was washed repeatedly by distilled water. Finally, the powder was treated in a N_2 flow at 473 K for 4 h. The prepared Co–MIL-101(Fe) were designed as x%wtCo–MIL-101(Fe), where x represents the predetermined cobalt ions content in mass fraction (different content of cobalt ions means different content of citric acid, mole ratio: $Co^{2+}/C_6H_8O_7 \cdot H_2O = 1{:}1.5$). Accordingly, the Co–MIL-101(Fe) catalysts were denoted as 4%wtCo–MIL-101(Fe), 6%wtCo–MIL-101(Fe), 8%wtCo–MIL-101(Fe), 10%wtCo–MIL-101(Fe), respectively. Similarly, Cu−MIL-101(Fe) catalysts were also synthesized in the same way.

Characterization

The crystallographic structures of the catalysts were carried on an X-ray diffractometer (XRD) D8 Advance X-ray Diffraction system and Bruker AXS with Cu Ka radiation ($\lambda = 0.15418$ nm). The dates were obtained in the 2θ range of 4°–60°. FTIR spectra were performed on a Nicolet 550 Fourier transform infrared in the range of 4000–400 cm^{-1}. Nitrogen adsorption/desorption isotherms were measured at 77 K using a Micrometrics ASAP 2020 surface area (BET) and porosimetry analyzer. Morphology images were also recorded on a Merlin scanning electron microscope (SEM). To investigate the presence of metal nanoparticles, Transmission electron microscopy (TEM) images were obtained on FEI Tecnai G2 F20 S-Twin operating at 200 kV. The contents of loaded metal were determined by inductively coupled plasma (ICP). AO7 concentration was detected using UV–vis spectrophotometry. Iron leaching of catalysts was evaluated by O phenanthroline spectrophotometric. Cobalt and copper leaching of catalysts was measured by atomic absorption spectrophotometer (AAS).

Adsorption performance for AO7 removal

To initiate the adsorption experiments, a 100 mL bottle equipped a weighed amount of adsorbent (0.02 g), followed by adding 100 mL of AO7 solution (0.01–0.1 mM/L, namely 3.5–35 mg/L). The test bottles were carried out in a room temperature shaker shaken at 180 rpm, 25 ± 0.2 °C. For a isotherm study, the adsorption proceeded for 1.5 h to reach apparent adsorption equilibrium. For a kinetics study, the adsorption was carried out at room temperature, and the supernatant was collected with a 0.45-μm membrane filter at different time intervals for the determination of unadsorbed AO7. The detection of AO7 was performed by UV–vis spectrophotometry ($\lambda = 484$ nm).

Catalytic performance for AO7 degradation

Batch experiments were carried out in a room temperature shaker shaken at 180 rpm, 25 ± 0.2 °C. In a typical procedure, catalyst was added to a bottle containing AO7 of 100 mL. Before adding the potassium persulfate, the suspension was rocked to establish the adsorption/desorption equilibrium. Afterwards, the persulfate activation was initiated by adding a given amount of potassium persulfate and without pH adjustment. At predetermined reaction time intervals, the 1-mL sample was extracted and immediately immersed in 1 mL ethanol solution to quench the further reaction, then measured.

The reusability of Co–MIL-101(Fe) and Cu–MIL-101(Fe) was investigated by means of recycling experiments. The catalysts were collected by centrifugal separation after reaction of 180 min, and then were washed with ethanol and water to remove adsorbed AO7. The next recycling experiment was re-initiated by adding a fresh solution of AO7 and PS.

Results and discussion

Analysis of catalysts characterization

XRD analysis

Figure 1 represents the XRD patters of the MIL-101(Fe) and metal modified MIL-101(Fe) with different Co or Cu

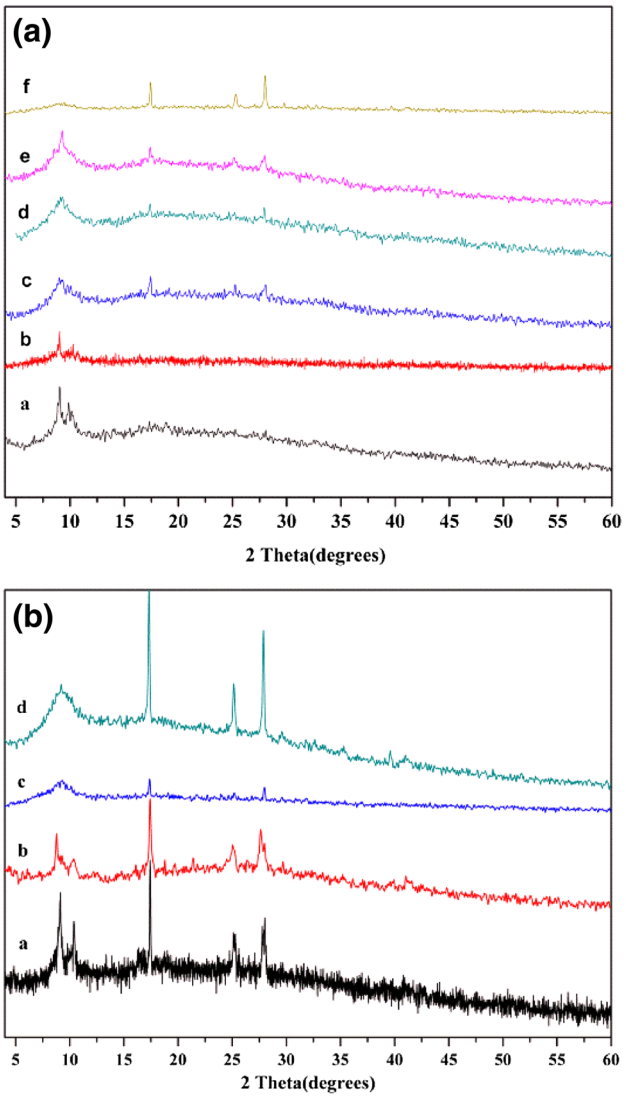

Fig. 1 XRD patters of materials: **a** *a* pure MIL-101(Fe), *b* MIL-101(Fe)(473 K), *c* 4%wtCo–MIL-101(Fe), *d* 6%wtCo–MIL-101(Fe), *e* 8%wtCo–MIL-101(Fe), *f* 10%wtCo–MIL-101(Fe). **b** *a* 4%wtCu–MIL-101(Fe), *b* 6%wtCu–MIL-101(Fe), *c* 8%wtCu–MIL-101(Fe), *d* 10%wtCu–MIL-101(Fe)

loadings. The distinct characteristic peaks of MIL-101(Fe) were observed at 2θ of 8.6°, 8.9°, 10.2°, 10.6° and 16.4°, which correspond to the previous reported articles (Skobelev et al. 2013; Tang et al. 2015). Modified MIL-101(Fe) also retained the main spectra of MIL-101(Fe) but with new defined peaks (2θ = 17.6°, 25.0°, 27.9°). However, in all modified samples, no new peaks associated to cobalt and copper particles were observed, suggesting that cobalt and copper particles may beyond the detection limit of the XRD or the cobalt and copper particles were highly dispersed. For comparison, unmodified MIL-101(Fe) was calcined at 473 K and characterized. The result showed the main spectra of MIL-101(Fe) were preserved and no new peaks were formed. An in-depth analysis of the XRD patters could produce some surprising findings. First, doping Co and Cu could induce the crystallographic defect in the MIL-101(Fe) for the main peaks ranging from 8° to 12° broaden and their intensity decreased dramatically. This observation has been reported by a relevant article (Qin et al. 2015). Second, Co doping caused much more crystallographic defect in the MIL-101(Fe) as compared to Cu doping. Third, the new formed peaks were related to both identity of metal and loading content. As shown, the intensity of new peaks of Co–MIL-101(Fe) seemed lower compared to Cu–MIL-101(Fe) and its new peaks were not shaped until the doped Co reaching a certain amount.

FTIR spectroscopy and Raman spectroscopy

Figure 2 records the FTIR spectrum of different samples. The characteristic IR peaks of pure MIL-101(Fe) were observed at around 1704, 1596, 1391, 1015, 747 and

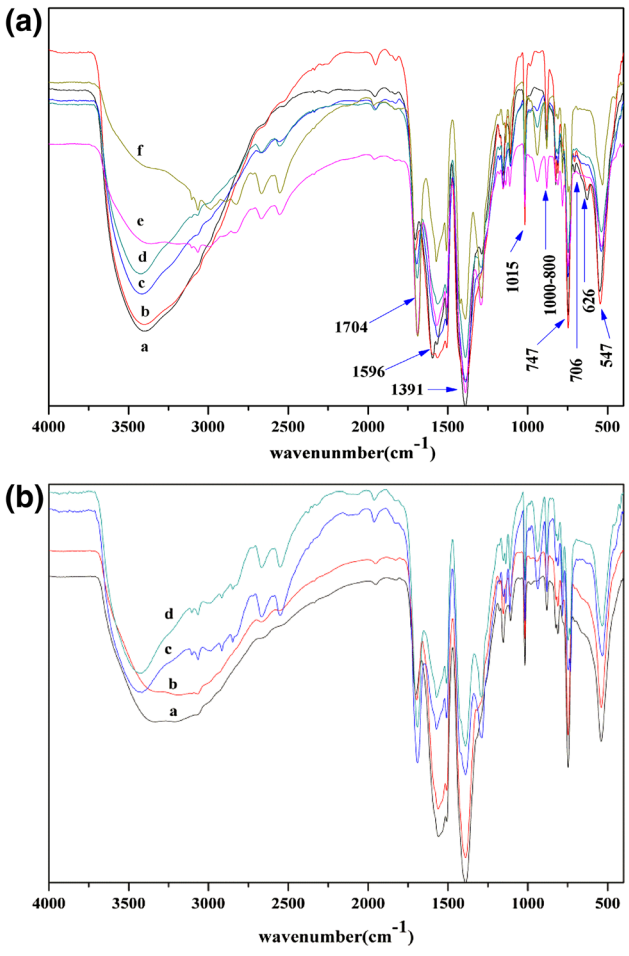

Fig. 2 FTIR spectra of materials: **a** *a* pure MIL-101(Fe), *b* 4%wtCu–MIL-101(Fe), *c* 6%wtCu–MIL-101(Fe), *d* 8%wtCu–MIL-101(Fe), *e* 10%wtCu–MIL-101(Fe); **b** *a* 4%wtCo–MIL-101(Fe), *b* 6%wtCo–MIL-101(Fe), *c* 8%wtCo–MIL-101(Fe), *d* 10%wtCo–MIL-101(Fe)

547 cm^{-1}, which matched well with the typical one reported in the literature (Tang et al. 2015). Metal-doped MIL-101(Fe) showed highly similar IR patters as that for MIL-101(Fe). Evidently, all of the samples exhibited a broad band in the region between 3600 and 3100 cm^{-1} ascribing to the presence of water. Compared with pure MIL-101(Fe), it is not difficult to read some spectrum changes of modified MIL-101 whether Co or Cu doping. First, the two peaks may be related to Fe–O bonds at 706 and 626 cm^{-1} were vanished due to the introduction of Co or Cu additives. In addition, the sharp peak at 1596 cm^{-1} assigned to C=O asymmetric vibration of carboxyl groups was slightly shifted to higher wavelength as compared to pure MIL-101(Fe). This phenomenon was due to the competing effects of metalation. Both Cu^{2+} and Co^{2+} can coordinate with carboxylic groups to form Cu–MOFs and Co–MOFs. It may pose a threat to metal iron sites for the reason that the interactions of Cu^{2+}(Co^{2+}) with the Fe–O center or the organic linker via π-complexation or a chelation process (Ebrahim and Bandosz 2013), and then more unsaturated iron nodes were exposed. It was possible that Cu^{2+}(Co^{2+}) was a new site of MIL-101(Fe). Moreover, the differences also could be recorded in the region of 1000–800 cm^{-1} assigned to C–H bending vibrations of benzene. Raman spectroscopy depicted in Fig. 3 also supports the fact Co or Cu additives successfully loaded in MIL-101(Fe), indicated by the newly formed peaks in the range from 200 to 500 cm^{-1} as compared to pure MIL-101(Fe). A new peak appeared at 1122 cm^{-1} may related to COO- of citric acid.

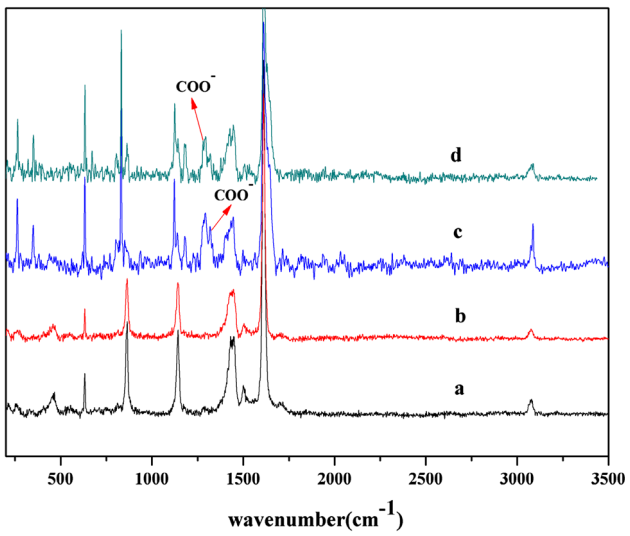

Fig. 3 Raman patters of materials: *a* pure MIL-101(Fe), *b* MIL-101(Fe)(473 K), *c* 6wt%Cu–MIL-101(Fe), *d* 6wt%Co–MIL-101(Fe)

N_2 physisorption analysis

Figure 4 shows the results of nitrogen adsorption/desorption isotherms of different catalysts. Table 1 displays the specific surface area, mesoporous volume and pore width of the samples. Metal contents on or within MIL-101(Fe) measured by ICP also are shown in Table 1. As expected, modified samples had a lower surface and a smaller pore volume than the pure one, which demonstrated that the addition of organometallic groups (copper citrate, cobalt citrate) do block the pores and do modify the structures of MIL-101(Fe). In addition, the higher the metal species loading was, the lower the specific surface area. Similar trend was observed in the mesoporous volume. On the contrary, the increases of pore width indicated the copper or cobalt species were partly formed in the surface of MIL-101(Fe). However, the results of ICP showed mass fraction of loaded Co or Cu ions were 0.150, 0.213, 0.155 and 0.205% for 4%wtCu–MIL-101(Fe), 6%wtCu–MIL-101(Fe), 4%wt Co–MIL-101(Fe) and 6%wtCo–MIL-

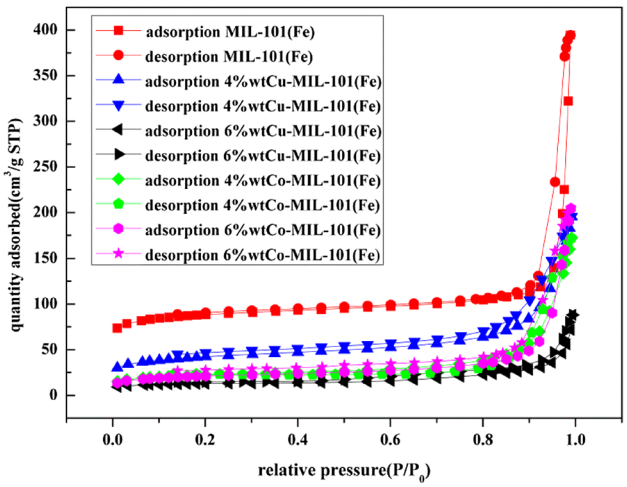

Fig. 4 Nitrogen adsorption/desorption isotherms of different catalysts

Table 1 BET surface area, mesoporous volume, pore width and metal content

Catalyst	BET surface area (m^2/g)	Mesoporous volume (cm^3/g)	Pore width (nm)	Loaded Me^{2+} (wt%)
Pure MIL-101(Fe)	300	0.307	4.1	
4%wtCu–MIL-101(Fe)	147	0.240	6.5	0.150
6%wtCu–MIL-101(Fe)	44	0.070	6.6	0.213
4%wtCo–MIL-101(Fe)	80	0.206	10.6	0.155
6%wtCo–MIL-101(Fe)	73	0.200	11.9	0.203

101(Fe) catalysts respectively, which pointed out only trace amounts of metal additives were successfully introduced as a result of the stronger completion from Fe(III) in terms of the coordination with BDC ligands (Binh et al. 2014).

SEM and TEM analysis

Figure 5 exhibits the morphology and particle size of the MIL-101(Fe), Cu–ML-101(Fe) and Co–MIL-101(Fe) catalysts. Pure MIL-101(Fe) displayed unusual octahedron morphology with average diameter of 800 nm ~1.5 μm. However, the SEM images of Cu–MIL-101(Fe) and Co–MIL-101(Fe) revealed great alterations in morphology and particle size. After loading Cu additives, the octahedron morphology appearance could be turned into roughened and irregular. Moreover, with the increase of Cu additives, a rod-like morphology of 2 μm in length has been shaped. From the images of Co–MIL-101(Fe), the roughened, disordered and partly crushed morphology was also formed. It seemed likely that Co additives generated a stronger influence on the octahedron morphology of MIL-101(Fe) than Cu additives did, which was also implied by the XRD results. Moreover, Co additives also made a rod-like morphology of 1–3 μm in length produced. The rod-like morphology was supported by the previous literature (Montazerolghaem et al. 2016), which indicated that Cu or Ni doping made rod-like morphology produced. The alterations in structure characteristics completely demonstrated the impact of competitive coordination between iron sites and doped metals to carboxylic groups in the BDC, and thus, more unsaturated iron sites could be initiated.

TEM images of 8%wtCo–MIL-101(Fe) were also characterized with FEI Tecnai G2 f20 s-twin, described in Fig. 6. Small Co nanoparticles with a size range of 3–5 nm embedded in MIL-101(Fe) were observed. Meanwhile, large Co nanoparticles with an average of 100 nm were also agglomerated on the surfaces of MIL-101(Fe).

Testing of catalysts adsorption and activity

Adsorption performance of catalysts

Prior to testing persulfate-activating performance, it was critical to examine whether the AO7 removal occurs simply by the catalyst adsorption. The adsorption isotherms of AO7 on pure MIL-101(Fe), 6%wtCo–MIL-101(Fe) and 6%wtCu–MIL-101(Fe) were shown in Fig. 7. The adsorption loadings, while the initial AO7 concentration was 35 mg/L, were 62.0, 22.8 and 17.5 mg/g for pure MIL-101(Fe), 6%wtCo–MIL-101(Fe) and 6wt%Cu–MIL-101(Fe), respectively. The result showed that the adsorption capacity of MIL-101(Fe) for AO7 was much bigger than 6%wtCo–MIL-101(Fe) and 6%wtCu–MIL-101(Fe). Furthermore, the adsorption data were analyzed with the help of Freundlich, which fits well with those three catalysts.

Fig. 5 SEM images of catalysts: **a** pure MIL-101(Fe), **b**, **c** 4%wtCu–MIL-101(Fe), **d**, **e** 6%wtCu–MIL-101(Fe), **f**, **g**: 4%wt Co–MIL-101(Fe), **h** 8%wt Co–MIL-101(Fe)

The effect of contact time for AO7 adsorption on 0.02 g catalysts for an initial AO7 concentration of 0.1 mM/L (35 mg/L) has been determined at 298 K. The adsorption loadings according to time are given in Fig. 8. The results indicated that maximum adsorption of AO7 was reached to the equilibrium in almost 30 min, which was used for all adsorption experiments. The kinetic parameters were obtained in light of the adsorption contact time experiments by pseudo-second order kinetic model. The pseudo-second-order kinetics model was feasible to describe the adsorption process of AOF on the pure MIL-101(Fe), 6%wtCo–MIL-101(Fe) and 6%wtCu–MIL-101(Fe).

Persulfate-activating performance of catalysts

Before the adding of PS, adsorption experiments were carried out in 30 min. Figure 9 shows the catalytic performance of pure MIL-101(Fe), 6%wtCu–MIL-101(Fe) and 6%wtCo–MIL-101(Fe). As expected, doping metal could significantly enhance the persulfate-activation compared to pure MIL-101(Fe). At the reaction time of 150 min, the removal rate of AO7 was about in 66, 92, 98% for MIL-101(Fe)/PS, 6wt%6%wtCu–MIL-101(Fe)/PS and 6wt%6%wtCo–MIL-101(Fe)/PS system, respectively. Interestingly, after adding sodium persulfate, the removal rate for 6%wtCu–MIL-101(Fe) and 6%wtCo–MIL-101(Fe) were not higher than that for MIL-101(Fe) until after reaction of 60 min. The stronger adsorption of MIL-101(Fe) may account for this, since the removal rate by MIL-101(Fe) adsorption has reached 37% within 30 min, which was greater than 6%wtCu–MIL-101(Fe) and 6wt%6%wtCo–MIL-101(Fe) adsorption. The results of Fig. 8 confirmed metal doping had a significantly positive effect on catalytic activities.

Influence of different Cu or Co loading contents

As discussed in the previous section, the presence of cobalt or copper additives greatly facilitated the activation of persulfate. Herein, batch experiments were conducted to examine the effects of different metal loading content on the AO7 removal. The results are depicted in Fig. 10. Take Co–MIL-101(Fe) catalyst for example, shown in Fig. 10a, the AO7 removal rate first increased with the increase of Co weight ratios, and then decreased when the Co–MIL-

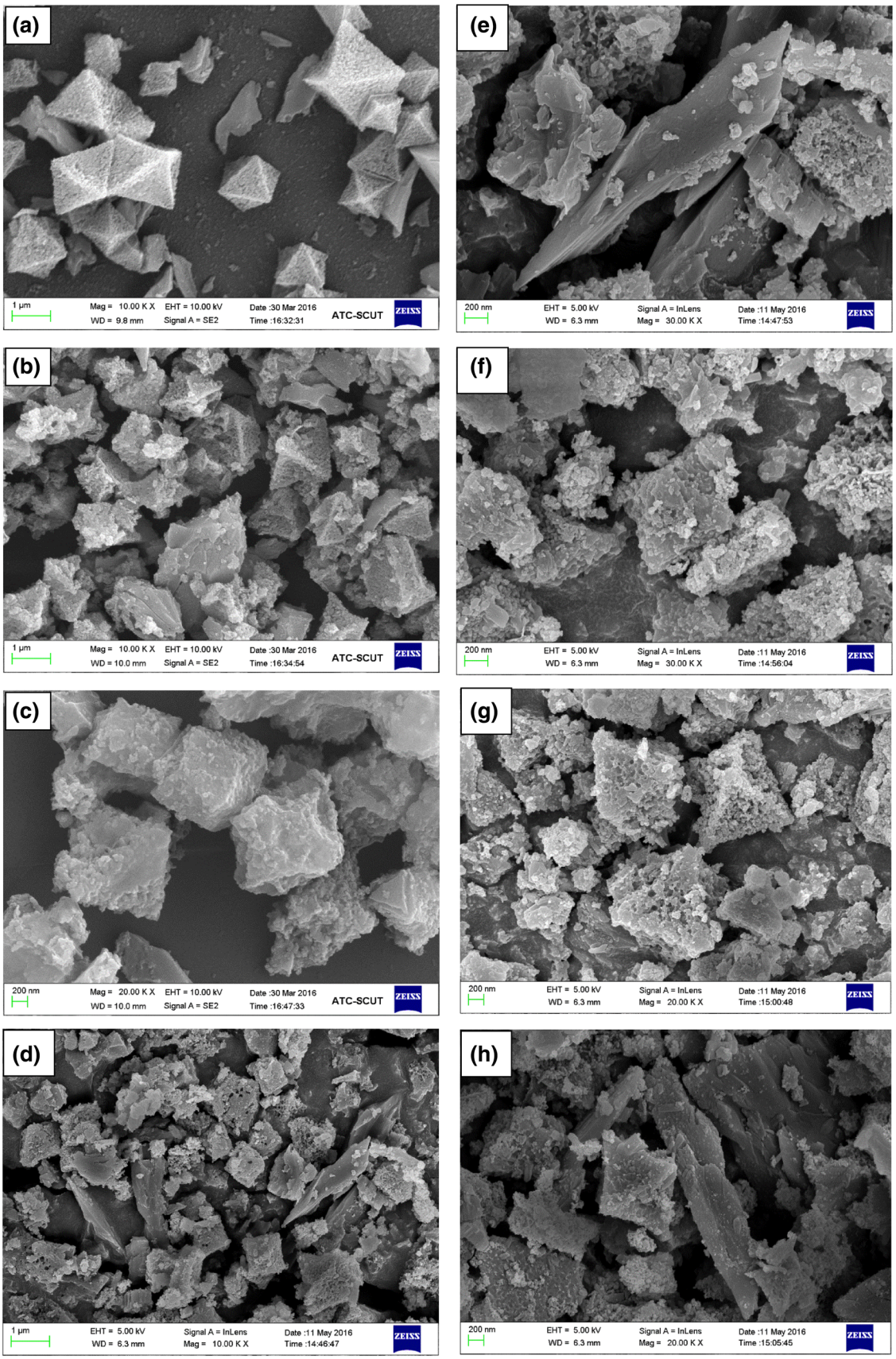
(a)
1 μm
Mag = 10.00 K X
EHT = 10.00 kV
WD = 9.8 mm
Signal A = SE2
Date :30 Mar 2016
Time :16:32:31
ATC-SCUT
ZEISS
(e)
200 nm
EHT = 5.00 kV
WD = 6.3 mm
Signal A = InLens
Mag = 30.00 K X
Date :11 May 2016
Time :14:47:53
ZEISS
(b)
1 μm
Mag = 10.00 K X
EHT = 10.00 kV
WD = 10.0 mm
Signal A = SE2
Date :30 Mar 2016
Time :16:34:54
ATC-SCUT
ZEISS
(f)
200 nm
EHT = 5.00 kV
WD = 6.3 mm
Signal A = InLens
Mag = 30.00 K X
Date :11 May 2016
Time :14:56:04
ZEISS
(c)
200 nm
Mag = 20.00 K X
EHT = 10.00 kV
WD = 10.0 mm
Signal A = SE2
Date :30 Mar 2016
Time :16:47:33
ATC-SCUT
ZEISS
(g)
200 nm
EHT = 5.00 kV
WD = 6.3 mm
Signal A = InLens
Mag = 20.00 K X
Date :11 May 2016
Time :15:00:48
ZEISS
(d)
1 μm
EHT = 5.00 kV
WD = 6.3 mm
Signal A = InLens
Mag = 10.00 K X
Date :11 May 2016
Time :14:46:47
ZEISS
(h)
200 nm
EHT = 5.00 kV
WD = 6.3 mm
Signal A = InLens
Mag = 20.00 K X
Date :11 May 2016
Time :15:05:45
ZEISS

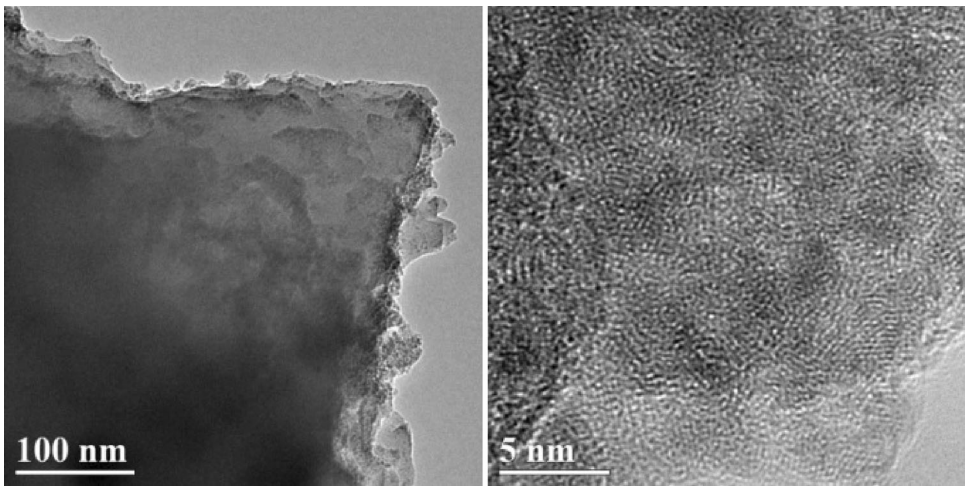

Fig. 6 TEM images of 8%wtCo–MIL-101(Fe) catalyst

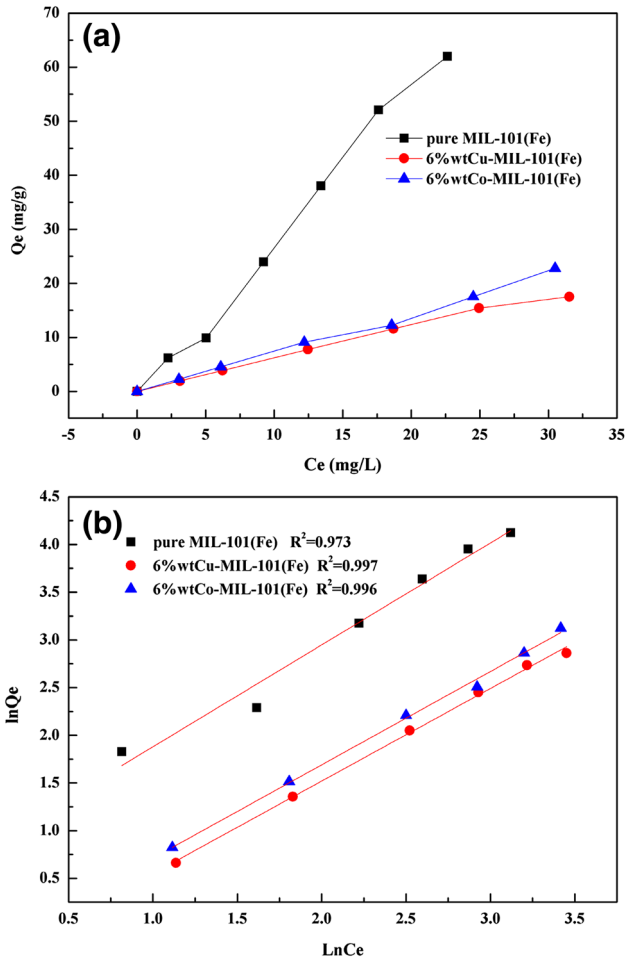

Fig. 7 AO7 adsorption on pure MIL-101(Fe), 6%wtCu–MIL-101(Fe) and 6%wtCo–MIL-101(Fe). **a** Adsorption isotherms; **b** Freundlich isotherm. Experimental conditions: $T = 25$ °C, catalysts dosage = 0.2 g/L, without pH adjustment

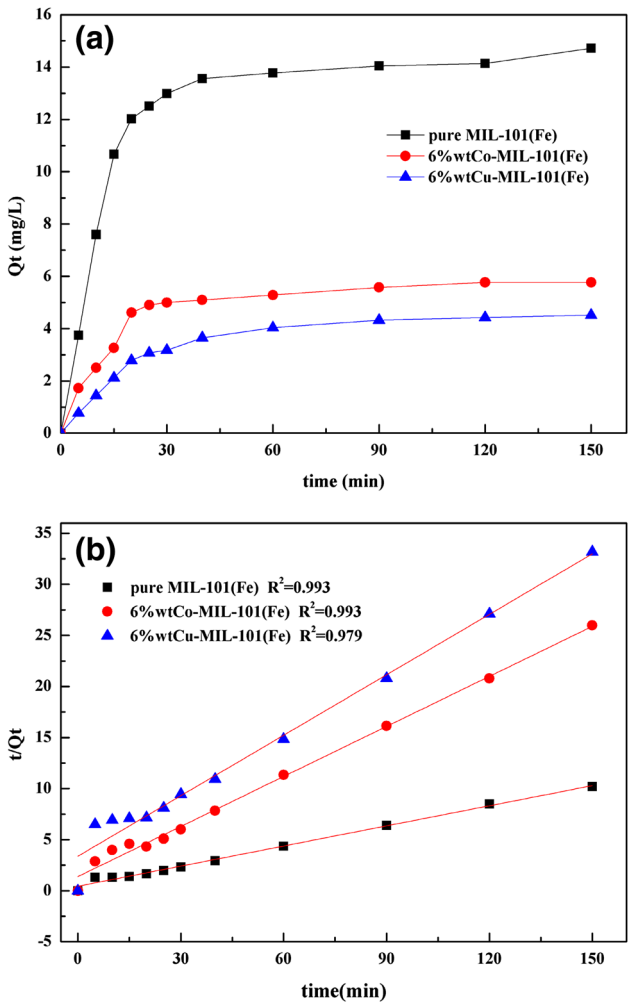

Fig. 8 Kinetics for the adsorption of AO7 on pure MIL-101(Fe), 6%wtCu–MIL-101(Fe) and 6%wtCo–MIL-101(Fe). **a** The effect of contact time; **b** pseudo-second-order. Experimental conditions: $T = 25$ °C, [AO7] = 0.1 mM, catalysts dosage = 0.2 g/L, without pH adjustment

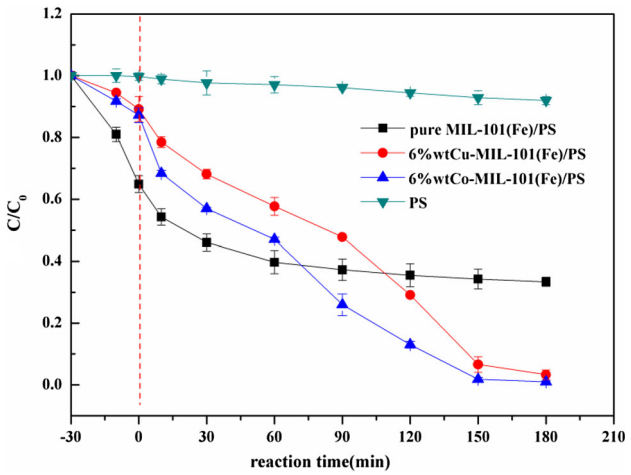

Fig. 9 AO7 removal in persulfate activation, with pure MIL-101(Fe), 6%wtCu–MIL-101(Fe) and 6%wtCo–MIL-101(Fe). Experimental conditions: [AO7] = 0.1 mM, [PS] = 8 mM, T = 25 °C, catalysts dosage = 0.2 g/L, without pH adjustment

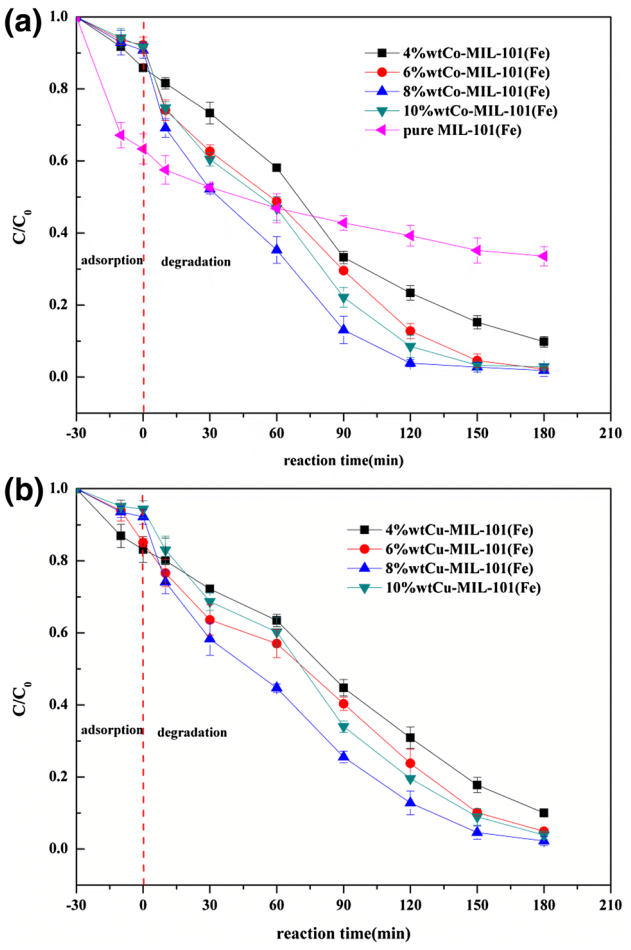

Fig. 10 Influence of metal loading content of catalysts on AO7 removal in persulfate activation. **a** Co–MIL-101(Fe); **b** Cu–MIL-101(Fe). Experimental conditions: [AO7] = 0.1 mM, [PS] = 8 mM, T = 25 °C, catalysts dosage = 0.3 g/L, without pH adjustment

101(Fe) weight ratios exceeded 8 wt%. Such trend was also shown in Cu–MIL-101(Fe) catalysts system. This phenomenon showed increasing the loading content of metals could improve catalytic capacity, but the catalytic capacity was inhibited when excessive metal deposited on MIL-101(Fe). It also indicated that loaded metal particles indeed played the role of new active species when persulfate activation, while high loading content caused the surface area decreased, inhibiting the interaction between catalyst and PS then lowering the catalysis performance. Though under the same prepared conditions, Co–MIL-101(Fe) catalysts manifested higher catalytic activity than Cu–MIL-101(Fe). The effects of the BET changes caused by metal additives can be excluded since both of them have a slight difference in adsorption to AO7 removal. However, the XRD and SEM results revealed that Co additives generated a stronger influence on the crystal and morphology of MIL-101(Fe) than Cu additives did, as ascribed above. Accordingly, Two reasons may be considered: (1) Metal nanoparticles loaded on or within the MIL-101(Fe) were participated in the persulfate activation then more sulfate radicals produced. (2) For Co–MIL-101(Fe) catalyst, the greater changes in crystal defect and disordered morphology probably bring much more active iron sites to exposure.

Influence of PS concentration

It is well-know that the performance of catalysis is strongly correlated to the PS concentration. This part focused on the influence of PS concentration ranging from 4 to 11 mM on the removal of AO7 while keeping the initial concentration of AO7 and catalyst dosage at constant 0.1 mM, 0.3 g/L, respectively, and without pH adjustment. Figure 11 showed the results obtained for catalytic ability with different PS concentration in each 8%wtCo–MIL-101(Fe)/PS and 8%wtCu–MIL-101(Fe)/PS system. It clearly revealed that the removal rate of AO7 both in the two systems increased with the increasing concentration of PS. For instance, at the reaction time of 90 min, the 8%wtCo–MIL-101(Fe) catalyst showed removal rate were 52, 57, 80, 88 and 91% corresponding to 4, 6, 8, 10 and 11 mM persulfate concentration. Nevertheless, as stated, the results of 8%wtCo–MIL-101(Fe)/PS showed the removal rate was just slightly enhanced when the PS concentration exceeded 8 mM. This phenomenon meant an increase in PS dosage could not continuously ensure an enhancement in persulfate activation, this phenomenon was supported by some literatures (Hori et al. 2007; Buxton et al. 1999; Salari et al.2009), which indicated inadequate use of $SO_4^{-\cdot}$ or the decay of $SO_4^{-\cdot}$ with $S_2O_8^{2-\cdot}$.

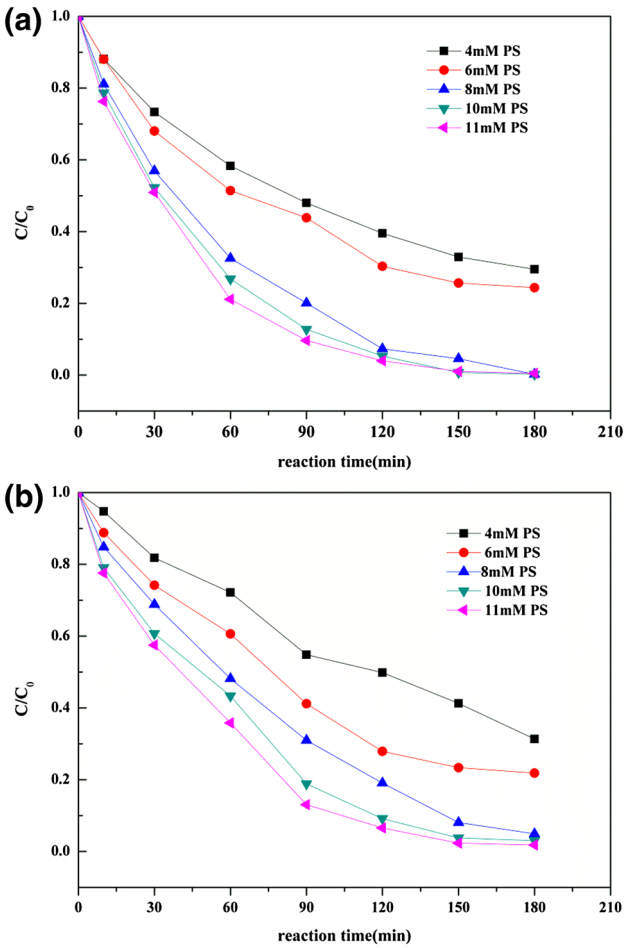

Fig. 11 Influence of PS concentration on AO7 removal in persulfate activation. **a** 8%wtCo–MIL-101(Fe); **b** 8%wtCu–MIL-101(Fe). Experimental conditions: [AO7] = 0.1 mM, T = 25 °C, catalysts dosage = 0.3 g/L, without pH adjustment

Determination of predominate radical species

Both $SO_4^{\cdot-}$ and $OH^{\cdot}$ are possibly responsible for the removal of AO7 since $SO_4^{\cdot-}$ in aqueous solution can happen inner-conversion reaction to generate $OH^{\cdot}$ (Hayon et al. 1972). Usually, for identification of predominate radical species in PS oxidation system, ethanol (ETOH) and tert-butanol (TBA) as radical scavengers are both together commonly used, considering that ETODH is an effective quencher for both $SO_4^{\cdot}$ and $OH^{\cdot}$ while TBA is an effective quencher for $OH^{\cdot}$ but not for $SO_4^{\cdot-}$. Radical scavengers with molar ratio 200:1 and 1000:1 (radical scavenger: AO7) were added into the persulfate-activating system, as illustrated in Fig. 12. Evidently, the removal rate of AO7 was slightly decreased in introduced TBA system (200:1) and just decreased a little more in molar ratio 1000:1. When ETOH:AO7 = 200:1, the catalytic ability was largely inhibited with the only 73% of AO7 removal rate, and more addition of ETOH resulted in

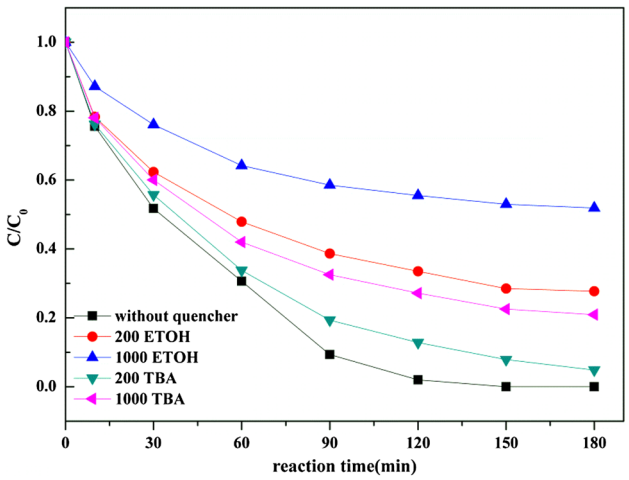

Fig. 12 Inhibiting influence of ETOH and TBA on AO7 removal in persulfate activation. Experimental conditions: 8%wtCo–MIL-101(Fe), [AO7] = 0.1 mM, T = 25 °C, catalysts dosage = 0.3 g/L, without pH adjustment

dramatical inhibition of persulfate activation, for the AO7 removal rate is below 50%. Thus, the radical inhibition experiments pointed out $SO_4^{\cdot-}$ was the dominant oxidative radical.

Reusability of Co–MIL-101(Fe) and Cu–MIL-101(Fe)

The stability of materials was evaluated by successive decolorization of AO7. The results obtained with the 8%wtCo–MIL-101(Fe) and 8%wtCu–MIL-101(Fe) are shown in Fig. 13. After reaction time of 180 min, the final AO7 removal rate in Co–MIL-101(Fe)/PS system were decreased to 96.6, 94.3, 88.6 and 73.8% for 1st, 2nd, 3rd and 4th use, respectively. It seemed the catalytic capacity reduced significantly. Cu–MIL-101(Fe) catalyst exhibited the same trend. The reduction of catalytic capacity was probably attributed to the following reasons: (1) the consumption of active sites including iron and doped metal caused the decrease in catalytic capacity. (2) adsorbed AO7 and some degradation products of AO7 still retained on the surface of catalysts, inhibiting the interaction of PS and metal active sites.

Metal leaching of catalysts

In an attempt to better understanding the consumption of metal sites, the metal leaching during the reaction time were investigated. Considering that the content of loaded metal was actually a little (ICP results) and the 0.010 mg/L of Co^{2+} for 6%wtCo–MIL-101(Fe) and 0.011 mg/L of Cu^{2+} for 6%wtCu–MIL-101(Fe) in final reaction solution tested by AAS, we were just focused on the iron leaching of catalysts by checking the dissolved iron concentration in

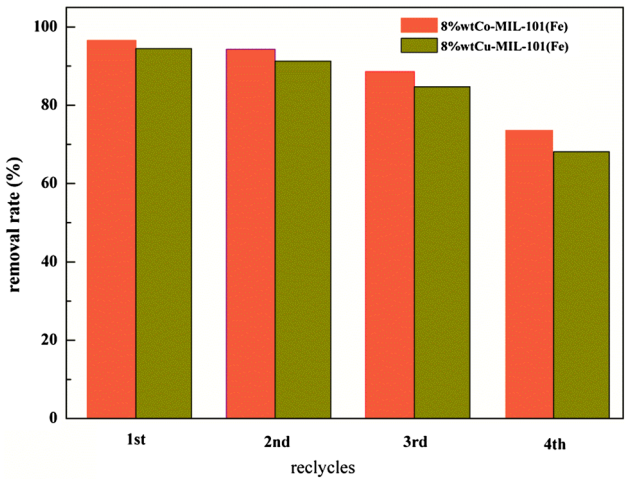

Fig. 13 AO7 removal rate by recycled catalysts (8%wtCo–MIL-101(Fe), 8%wtCo–MIL-101(Fe)). Experimental conditions: [AO7] = 0.1 mM, T = 25 °C, catalysts dosage = 0.3 g/L, without pH adjustment

aqueous solution. Figure 14 showed the results of dissolved iron of different catalysts, MIL-101(Fe), 4wt%Cu–MIL-101, 6wt%Cu–MIL-101, 4%wtCo–MIL-101 and 6%wtCo–MIL-101. In all cases, the concentration of dissolved iron increased along with the increase of AO7 removal rate. On the one hand, regardless of the identity of metal additives, the more introducing of metal additives, the more removal rate of AO7 and then the more leaching amounts of iron. On the other hand, when introduced the same amounts of metal additives, the Co–MIL-101 catalysts showed better catalytic performance and more iron leaching than Cu–MIL-101. It seems likely that there is close relationship between catalytic performance and iron leaching.

Hence, we wonder the persulfate activation is heterogeneous reaction by solid catalysts or homogeneous reaction induced by dissolved iron. To address this problem, we designed an experiment as shown below: First, distilled water of 100 mL was adjusted with H_2SO_4 (pH value kept the same with the system of adding PS above); Second, catalysts were immersed in the distilled water and rocked in a shaker; Then, at predetermined reaction time intervals, 0.5 mL of solution was drawn out for measuring dissolved iron; After 3 h, the solution through a 0.45-μm membrane filter was used as homogeneous catalyst to remove AO7 with adding sodium persulfate. The results of dissolved iron were described by Fig. 15a and the corresponding removal of AO7 are shown by Fig. 15b. From the two

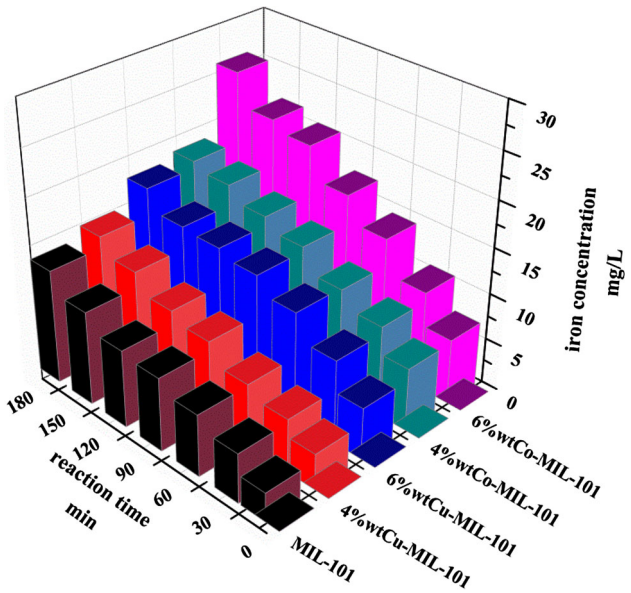

Fig. 14 Investigation of iron leaching of catalysts during reaction time in PS activation. Experimental conditions: [AO7] = 0.1 mM, [PS] = 8 mM, catalyst dosage = 0.3 g/L, T = 25 °C, without pH adjustment

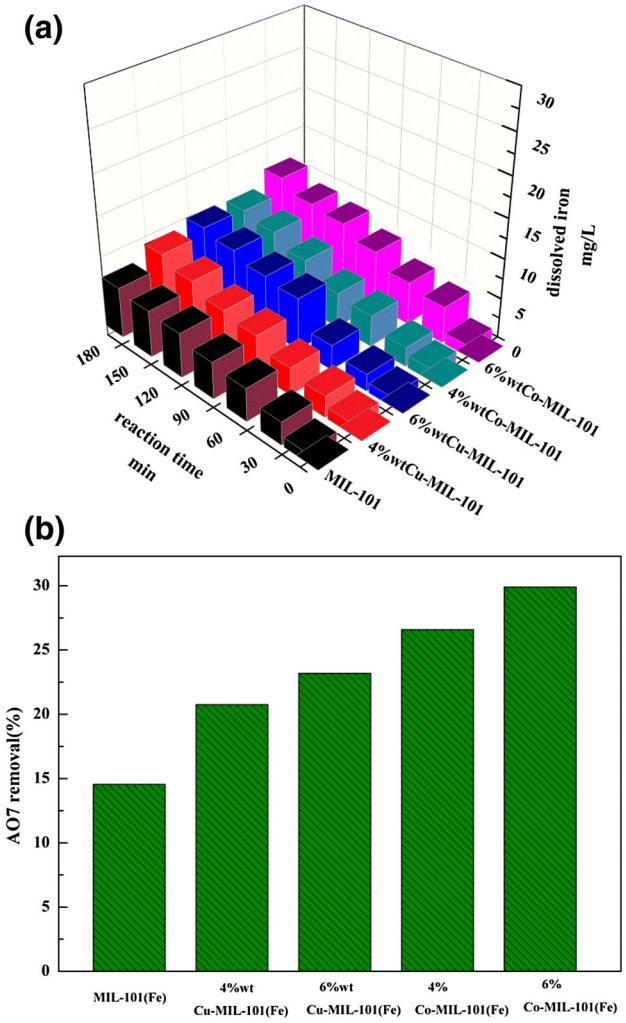

Fig. 15 **a** Investigation of iron leaching of catalysts in acid solution without PS. Experimental conditions: catalysts = 0.3 g/L, 100 mL H20, T = 25 °C. **b** AO7 removal corresponding to the iron leaching of (**a**)

pictures, we found the leaching of iron was much lower than PS activation system and the AO7 removal rate was also undesirable. In addition, the trend of leaching amount was in agreement with that of containing PS system (illustration above). Naturally, reasonable conclusions can be made: (1) Iron leaching was induced by the impact of interaction between active iron sites of catalysts and persulfate instead of its instability in solution. The stronger catalytic action resulted in the defects of Fe(III). (2) The persulfate activation was heterogeneous reaction taken place on catalyst surface rather than in homogeneous solution containing leached iron. (3) The alteration in structure characteristics may result in the difference of leached iron. For unmodified MIL-101(Fe), the amount of leached iron was much lower than modified ones. While Co–MIL-101 with greater alterations showed more iron amounts as compared with Cu modification. It was assumed to be the result of more active iron sites induced by greater structure alterations.

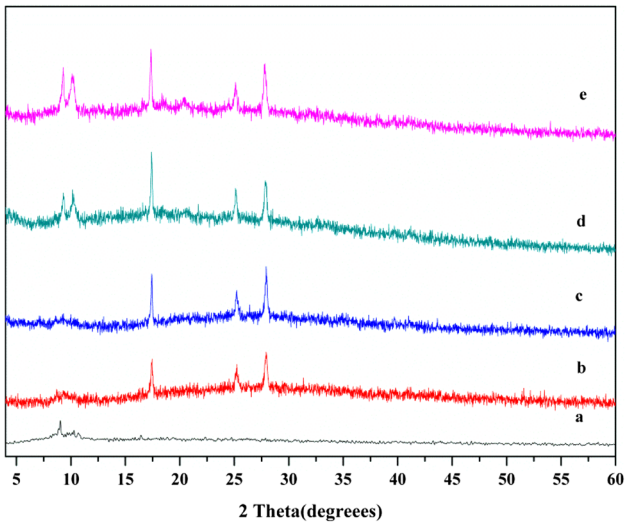

Fig. 16 XRD patters of used catalysts: *a* MIL-101(Fe), *b* 4%wtCo–MIL-101(Fe), *c* 6wt%6%wtCo–MIL-101(Fe), *d* 4%wtCu–MIL-101(Fe), *e* 6%wtCu–MIL-101(Fe)

Possible catalytic mechanism

The role of metal additives on catalysts

To our knowledge, many researchers have successfully integrated other metal ions (Mg^{2+}, Ni^{2+}, Cu^{2+}, Fe^{3+}, Ce^{3+}) into MOFs, although the original XRD patterns changed (Qin et al. 2015; Wen et al. 2015; Zhou et al. 2016) and octahedron morphology became indistinct and disordered (Ebrahim and Bandosz 2013; Wen et al. 2015), which may be ascribed to the competition between the doped metal ions and inherent metal centers to link the carboxylic groups in the BDC and thus was reflected in the crystalline structure. The competed interaction brought inherent saturated iron sites to unsaturated. What is more, metal additives as new active sites played the role of activating PS to produce sulfate radicals. Nevertheless, the ICP result suggested the loaded content of metal was below 0.3 wt% actually. It was reasonable that the reaction between new active sites with PS was not fundamental reason for the enhancement of catalysis. This may be due to that Co^{2+} or Cu^{2+} induced crystal defect and changed morphology appearance then more unsaturated iron sites to be exposure. In addition, metal-modified MIL-101(Fe) showed lower adsorption to AO7, this result indicated less adsorption, the more activation. We attributed this phenomenon to adsorptive competition between PS and AO7 to active metal centers. More free radicals benefited from more adsorption of PS.

To further explain the difference of catalytic performance, the crystalline structure and surface properties of catalysts after activation reaction were examined by XRD and SEM. As shown in Fig. 16, the XRD patters appeared obvious alteration after catalytic reaction. MIL-101(Fe) remained its original patters at the same angles except for a little decrease in intensity. However, the peaks of Co–MIL-101(Fe) and Cu–MIL-101(Fe) catalysts were different. First, the peaks intensity at $2\theta = 17.6°$, 25.0°, 27.9° were enhanced in Co–MIL-101(Fe) catalysts. Second, the characteristic peaks at the range of 8°–12° were disappeared in Co–MIL-101(Fe) patters, while still retained in Cu–MIL-101(Fe) patters. SEM images in Fig. 17 pointed out entirely different in morphology. Pure MIL-101(Fe) maintained its octahedron morphology along with a little loss in structure. The morphology of Cu–MIL-101(Fe) totally turned into rod-like particles with uneven size distribution of 2–6 μm. While the SEM images of Co–MIL-101(Fe) demonstrated that lamellar-like and flower-like structures were successfully shaped. The morphology of Co–MIL-101(Fe) and Cu–MIL-101(Fe) catalysts were quite different to that before reaction. The higher activity of Co–MIL-101(Fe) for PS activation was assumed to be the result of Co additives causing substantial and positive changes in crystal and morphology.

Unsaturated iron sites for persulfate activation

In terms of the proposed mechanisms in literatures (Li et al. 2016; Lu et al. 2016; Liang et al. 2009; Ahmad et al. 2012; Liu et al. 2014), Fe^{3+} can activate persulfate to produce $SO_4^{-\cdot}$ for contaminant degradation. Here, our synthesized catalysts contained much more active ≡ Fe(trivalent) sites, which could excite persulfate to form free radicals in the same manner like homogeneous catalytic reaction of Fe^{3+}. The degradation mechanism of AO7 by metal-modified catalysts was illustrated through Eqs. (1)–(4).

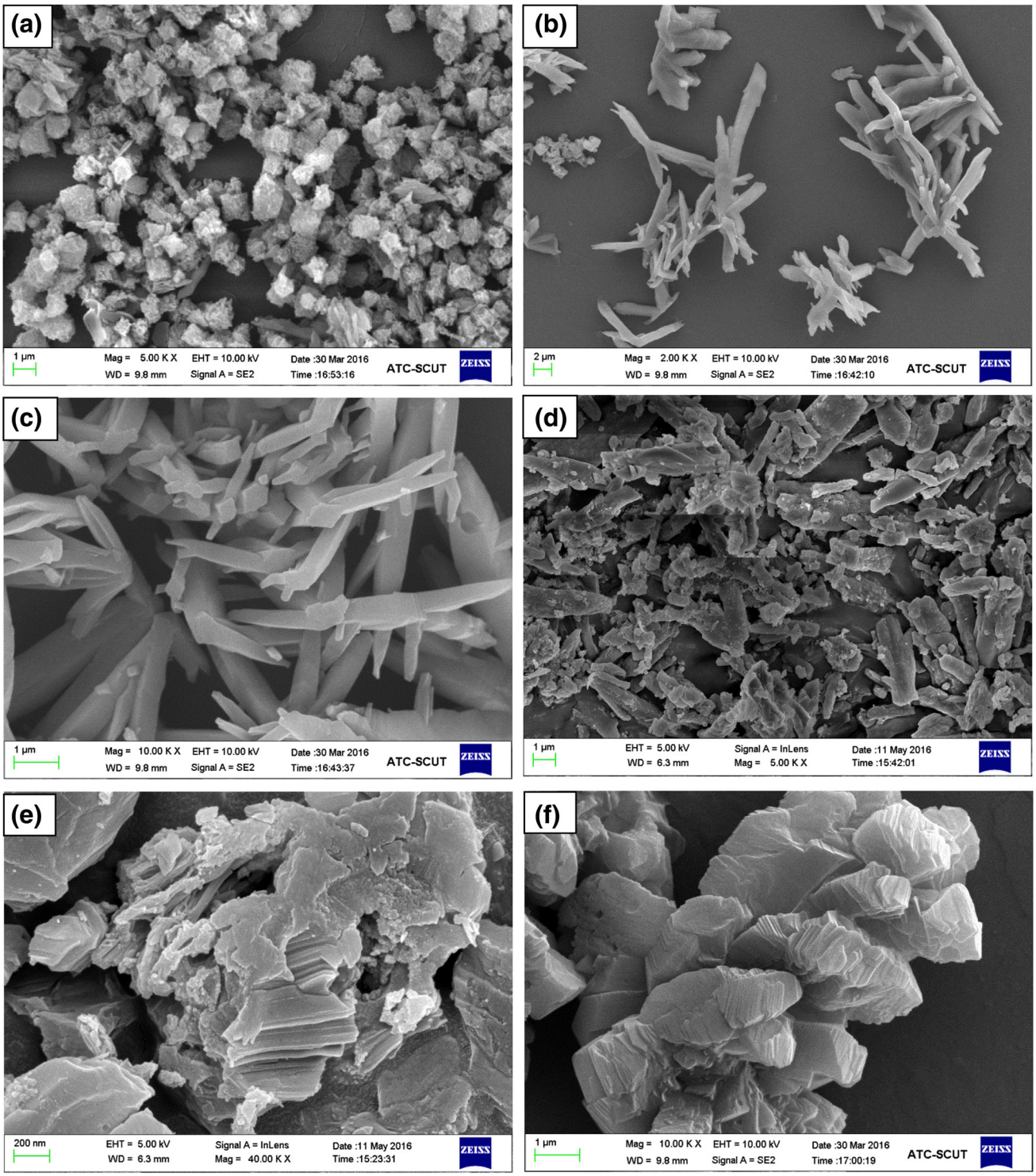

Fig. 17 SEM images of used catalysts: **a** MIL-101(Fe); **b**, **c** Cu–MIL-101(Fe); **d**, **e**, **f** Co–MIL-101(Fe)

First, the active ≡ Fe(III) react with PS to form ≡ Fe(II) and $S_2O_8^{\cdot-}$. After iron sites reduced, plenty of $SO_4^{\cdot-}$ were created via the reaction between ≡ Fe(II) and $S_2O_8^{2-}$. Then AO7 was degraded by the $SO_4^{\cdot-}$. The reaction between $SO_4^{\cdot-}$ and H_2O also produced the $OH^{\cdot}$. In addition, new active sites created by Cu(II) and Co(II) also participated in the catalytic activity (Formula omitted). The fact that persulfate oxidized by ≡ Fe(III) and reduced by ≡ Fe(II) is analogous to the mechanism of H_2O_2 in Fenton system.

$$\equiv Fe^{3+} + S_2O_8^{2-} \rightarrow \equiv Fe^{2+} + S_2O_8^{-}\cdot, \quad (1)$$

$$\equiv Fe^{2+} + S_2O_8^{2-} \rightarrow \equiv Fe^{3+} + SO_4^{-}\cdot + SO_4^{2-}, \quad (2)$$

$$SO_4^{-}\cdot + H_2O \rightarrow \cdot OH + H^+ + SO_4^{2-}, \quad (3)$$

$$AO7 + SO_4^{-}\cdot \rightarrow CO_2 + H_2O + \cdots \quad (4)$$

Conclusions

The study was the first attempt to use MIL-101(Fe) doped with Co and Cu as heterogeneous catalysts to degrade AO7 in the presence of persulfate. XRD, Raman, SEM and TEM analysis all revealed metal additives were successfully introduced into MIL-101(Fe). Removal rate of AO7 in 150 min reached 66, 92, 98% for pure MIL-101(Fe), 6%wtCu–MIL-101(Fe) and 6%wtCo–MIL-101(Fe), respectively. It was found that doping metals was capable of greatly enhancing the performance of persulfate activation. The reason for this was attributed to the role that metal additives played. First, less important, doped metals (Co and Cu) behaved as active species to produce sulfate radicals. Second, doping metals decreased specific surface area of MIL-101(Fe) and showed lower adsorption to AO7 which could be beneficial to persulfate adsorption and then more sulfate radicals were produced. Third, more critically, the changes of crystalline structure and morphology appearance were mainly responsible for the catalytic enhancement, which was due to the competed coordination between the doped metal ions with saturated iron ions to link the carboxylic groups in the BDC and thus an increasing number of active Fe sites were produced. What is more, this study allowed the comparison of the catalytic ability of Co and Cu additives with different percentages. Our research showed Co additives brought about better positive effect in PS activation than that of Cu additives, this may due to the greater changes in crystalline structure and morphology appearance caused by Co additives and then initiate more unsaturated iron sites. However, how metal additives effect on crystalline structure and morphology characteristic and what relationship between unsaturated iron sites and morphology characteristic remain unclear. Some researches need to be further investigated. Nevertheless, as stated, the MIL-101(Fe) doped with Co or Cu indeed showed excellent prospects in water treatment.

Acknowledgements This research has been supported by National Natural Science Foundation of China (No. 31570568), High-level Personnel Foundation of Guangdong Higher Education Institutions (2013), State key laboratory of Pulp and Paper Engineering in China (No. 201535). The authors are grateful to all the anonymous reviewers for their insightful comments and suggestions.

References

Ahmad M, Teel AL, Furman OS, Reed JI, Watts RJ (2012) Oxidative and reductive pathways in iron-ethylenediaminetetraacetic acid-activated persulfate systems. J. Environ Eng-Asce 138:411–418. doi:10.1061/(ASCE)EE.1943-7870.0000496

Ai LH, Zhang CH, Li LL, Jiang J (2014) Iron terephthalate metal-organic framework: revealing the effective activation of hydrogen peroxide for the degradation of organic dye under visible light irradiation. Appl Catal B Environ 148:191–200. doi:10.1016/j.apcatb.2013.10.056

Alaerts L, Séguin E, Poelman H, Thibault-Starzyk F, Jacobs PA, De Vos D (2006) Probing the Lewis acidity and catalytic activity of the metal-organic framework [Cu-3(btc)(2)] (BTC = benzene-1,3,5-tricarboxylate). Chem Eur J 12:7353–7363. doi:10.1002/chem.200600220

Binh NT, Tien DM, Giang LTK, Khuyen HT, Huong NT, Huong TT, Lam TD (2014) Study on preparation and characterization of MOF based lanthanide doped luminescent coordination polymers. Mater Chem Phys 143:946–951. doi:10.1016/j.matchemphys.2013.09.048

Buxton GV, Bydder M, Salmon GA (1999) The reactivity of chlorine atoms in aqueous solution - Part II. The equilibrium SO_4^{-} + Cl- reversible arrow $Cl^{-\cdot}$ + SO_4^{2-}. Phys Chem Chem Phys 1:269–273. doi:10.1039/A807808D

Ebrahim AM, Bandosz TJ (2013) Ce(III) doped Zr-based MOFs as excellent NO_2 adsorbents at ambient conditions. ACS Appl Mater Int 5:10565–10573. doi:10.1021/am402305u

Fang DD, Gao J, Dionysiou DD, Liu C, Zhou DM (2013) Activation of persulfate by quinones: free radical reactions and implication for the degradation of PCBs. Environ Sci Technol 47:4605–4611. doi:10.1021/es400262n

Fei HH, Shin JW, Meng YS, Adelhardt M, Sutter J, Meyer K, Cohen SM (2014) Reusable oxidation catalysis using metal-monocatecholato species in a robust metal-organic framework. J Am Chem Soc 136:4965–4973. doi:10.1021/ja411627z

Gayathri P, PraveenaJuliyaDorathi R, Palanivelu K (2009) Sonochemical degradation of textile dyes in aqueous solution using sulphate radicals activated by immobilized cobalt ions. UltrasonSonochem. 17:566–571. doi:10.1016/j.ultsonch.2009.11.019

Hayon E, Treinin A, Wilf J, Am J (1972) Chem Soc doi:10.1021/ja00756a009

Hori H, Yamamoto A, Koike K ,Kutsuna S , Osaka I, Arakawa R (2007) Photochemical decomposition of environmentally persistent short-chain perfluorocarboxylic acids in water mediated by iron(II)/(III) redox reactions.Chemosphere 68:572-578. doi:10.1016/j.chemosphere.2006.12.038

Hwang YK, Hong DY, Chang JS, Jhung SH, Sea YK, Kim J, Vimont A, Daturi M, Serre C, Férey G (2008) Amine grafting on coordinatively unsaturated metal centers of MOFs: consequences for catalysis and metal encapsulation. Angew Chem Int Ed 47:4144–4148. doi:10.1002/anie.200705998

Klavarioti M, Mantzavinos D, Kassinos D (2009) Removal of residual pharmaceuticals from aqueous systems by advanced oxidation processes. Environ Int 35:402–417. doi:10.1016/j.envint.2008.07.009

Kurniawan TA, Lo W, Chan GSY (2006) Radicals-catalyzed oxidation reactions for degradation of recalcitrant compounds from landfill leachate. Chem Eng J 125:35–57. doi:10.1016/j.cej.2006.07.006

Lei Q, Li ZW, Xu ZH, Guo XW, Zhang GL (2015) Organic-acid-directed assembly of iron-carbon oxides nanoparticles on coordinatively unsaturated metal sites of MIL-101 for green photochemical oxidation. Appl Catal B Environ 179:500–508. doi:10.1016/j.apcatb.2015.06.001

Li JR, Kuppler RJ, Zhou HC (2009) Selective gas adsorption and separation in metal-organic frameworks. Chem Soc Rev 38:1477–1504. doi:10.1039/b802426j

Li Y, Li H, Zhang J, Guan GX, Lan YQ (2014) Efficient degradation of congo red by sodium persulfate activated with zero-valent zinc. Water Air Soil Pollut. doi:10.1007/s11270-014-2121-8

Li XH, Guo WL, Liu ZH, Wang RQ, Liu H (2016) Fe-based MOFs for efficient adsorption and degradation of acid orange 7 in aqueous solution via persulfate activation. Appl Surf Sci 369:130–136. doi:10.1016/j.apsusc.2016.02.037

Liang CJ, Liang CP, Chen CC (2009) pH dependence of persulfate activation by EDTA/Fe(III) for degradation of trichloroethylene. J Contam Hydrol 106:173–182. doi:10.1016/j.jconhyd.2009.02.008

Liang HY, Zhang YQ, Huang SB, Hussain I (2013) Oxidative degradation of p-chloroaniline by copper oxidate activated per sulfate. Chem Eng J 218:384–391. doi:10.1016/j.cej.2012.11.093

Liang RW, Jing FF, Shen LJ, Qin N, Wu L (2015) MIL-53(Fe) as a highly efficient bifunctional photocatalyst for the simultaneous reduction of Cr(VI) and oxidation of dyes. J Hazard Mater 287:364–372. doi:10.1016/j.jhazmat.2015.01.048

Lin YT, Liang CJ, Chen JH (2011) Feasibility study of ultraviolet activated persulfate oxidation of phenol. Chemosphere 82:1168–1172. doi:10.1016/j.chemosphere.2010.12.027

Lin KYA, Chang HA, Hsu CJ (2015) Iron-based metal organic framework, MIL-88A, as a heterogeneous persulfate catalyst for decolorization of Rhodamine B in water. RSC Adv 5:32520–32530. doi:10.1039/C5RA01447F

Lin XM, Ma YW, Wan JQ, Wang Y (2017) LiCoPO4 (LCP) as an effective peroxymonosulfate activator for degradation of diethyl phthalate in aqueous solution without controlling pH: efficiency, stability and mechanism. Chem Eng J 315:304–314. doi:10.1016/j.cej.2017.01.036

Liu HZ, Bruton TA, Doyle FM, Sedlak DL (2014) In situ chemical oxidation of contaminated groundwater by persulfate: decomposition by Fe(III)- and Mn(IV)-containing oxides and aquifer materials. Environ Sci Technol 48:10330–10336. doi:10.1021/es502056d

Llabrés I, Xamena FX, Corma A, Garcia H (2007) Applications for metal-organic frameworks (MOFs) as quantum dot semiconductors. J Phys Chem C 111:80–85. doi:10.1021/jp063600e

Lu YS, Yang XX, Xu L, Wang Z, Xu YE, Desalin Qian GR (2016) Sulfate radicals from Fe^{3+}/persulfate system for Rhodamine B degradation. Water Treat 57:29411–29420. doi:10.1080/19443994.2016.1148641

Lv HL, Zhao HY, Cao TC, Qian L, Wang YB, Zhao GH (2015) Efficient degradation of high concentration azo-dye wastewater by heterogeneous Fenton process with iron-based metal-organic framework. J Mol Catal A Chem 400:81–89. doi:10.1016/j.molcata.2015.02.007

Montazerolghaem M, Aghamiri SF, Tangestaninejad S, Talaie MR (2016) A metal-organic framework MIL-101 doped with metal nanoparticles (Ni and Cu) and its effect on CO_2 adsorption properties. RSC Adv 6:632–640. doi:10.1039/C5RA22450K

Nguyen MTH, Nguyen QT (2014) Efficient refinement of a metal-organic framework MIL-53(Fe) by UV–vis irradiation in aqueous hydrogen peroxide solution. J Photochem Photobiol A 288:55–59. doi:10.1016/j.jphotochem.2014.05.006

Nie MH, Yang Y, Zhang ZJ, Yan CX, Wang XN, Li HJ, Dong WB (2014) Degradation of chloramphenicol by thermally activated persulfate in aqueous solution. Chem Eng J 246:373–382. doi:10.1016/j.cej.2014.02.047

Oh SY, Kim HW, Park JM, Park HS, Yoon C (2009) Oxidation of polyvinyl alcohol by persulfate activated with heat, Fe^{2+}, and zero-valent iron. J Hazard Mater 168:346–351. doi:10.1016/j.jhazmat.2009.02.065

Oh SY, Kang SG, Chiu PC (2010) Degradation of 2,4-dinitrotoluene by persulfate activated with zero-valent iron. Sci Total Environ 408:3464–3468. doi:10.1016/j.scitotenv.2010.04.032

Pu MJ, Ma YW, Wan JQ, Wang Y, Huang MZ, Chen YM (2015) Fe/S doped granular activated carbon as a highly active heterogeneous persulfate catalyst toward the degradation of Orange G and diethyl phthalate. J. Colloid Interf. Sci. 418:330–337. doi:10.1016/j.jcis.2013.12.034

Qin L, Li ZW, Xu ZH, Guo XW, Zhang GL (2015) Organic-acid-directed assembly of iron-carbon oxides nanoparticles on coordinatively unsaturated metal sites of MIL-101 for green photochemical oxidation. Appl Catal B Environ 179:500–508. doi:10.1016/j.apcatb.2015.06.001

Rocca JD, Liu DM, Lin WB (2011) Nanoscale metal-organic frameworks for biomedical imaging and drug delivery. Acc Chem Res 44:957–968. doi:10.1021/ar200028a

Salari D, Niaei A, Aber S, Rasoulifard MH (2009) The photooxidative destruction of Cl Basic Yellow 2 using UV/S2O82- process in a rectangular continuous photoreactor. J Hazard Mater 166:61–66. doi:10.1016/j.jhazmat.2008.11.039

Shen LJ, Liang SJ, Wu WM, Liang RW, Wu L (2013) Multifunctional NH2-mediated zirconium metal-organic framework as an efficient visible-light-driven photocatalyst for selective oxidation of alcohols and reduction of aqueous Cr(VI). Dalton Trans 42:13649–13657. doi:10.1039/C3DT51479J

Skobelev IY, Sorokin AB, Kovalenko KA, Fendin VP, Kholdeeva OA (2013) Solvent-free allylic oxidation of alkenes with O-2 mediated by Fe-and Cr-MIL-101. J Catal 298:61–69. doi:10.1016/j.jcat.2012.11.003

Sun C, Zhou R, Jianan E, Sun JQ, Ren HJ (2015) Magnetic $CuO@Fe_3O_4$ nanocomposite as a highly active heterogeneous catalyst of persulfate for 2,4-dichlorophenol degradation in aqueous solution. RSC Adv 5:57058–57066. doi:10.1039/C5RA09821A

Tang J, Yang M, Wang J, Dong JJ, Wang G (2015) Heterogeneous Fe-MIL-101 catalysts for efficient one-pot four-component coupling synthesis of highly substituted pyrroles. New J Chem 39:4919–4923. doi:10.1039/C5NJ00632E

Taylor-Pashow KML, Rocca JD, Xie ZG, Tran S, Lin WB (2009) Postsynthetic modifications of iron-carboxylate nanoscale metal-organic frameworks for imaging and drug delivery. J Am Chem Soc 131:14261–14263. doi:10.1021/ja906198y

Vallejo M, Román MFS, Irabien A (2015) Overview of the PCDD/Fs degradation potential and formation risk in the application of advanced oxidation processes (AOPs) to wastewater treatment. Chemosphere 118:44–56. doi:10.1016/j.chemosphere.2014.05.077

Waldemer RH, Tratnyek PG, Johnson RL, Nurmi JT (2007) Oxidation of chlorinated ethenes by heat-activated persulfate: kinetics and products. Environ Sci Technol 41:1010–1015. doi:10.1021/es062237m

Wen MC, Kuwahara Y, Mori K, Zhang DQ, Li HX, Yamashita H (2015) Synthesis of Ce ions doped metal-organic framework for promoting catalytic H-2 production from ammonia borane under visible light irradiation. J Mater Chem A. 3:14134–14141. doi:10.1039/C5TA02320C

Wu F, Qiu LG, Ke F, Jiang X (2013) Copper nanoparticles embedded in metal-organic framework MIL-101(Cr) as a high performance catalyst for reduction of aromatic nitro compounds. Inorg Chem Commun 32:5–8. doi:10.1016/j.inoche.2013.03.003

Zhang CH, Ai LH, Jiang J (2015) Solvothermal synthesis of MIL-53(Fe) hybrid magnetic composites for photoelectrochemical water oxidation and organic pollutant photodegradation under visible light. J Mater Chem 3:3074–3081. doi:10.1039/C4TA04622F

Zhao HY, Qian L, Lv HL, Wang YB, Zhao GH (2015) Introduction of a Fe_3O_4 core enhances the photocatalytic activity of MIL-100(Fe) with tunable shell thickness in the presence of H_2O_2. Chemicalchem. 7:4148–4155. doi:10.1002/cctc.201500801

Zhou HC, Long JR, Yaghi OM (2012) Introduction to metal-organic frameworks. Chem Rev 112:673–674. doi:10.1021/cr300014x

Zhou ZY, Mei L, Ma C, Xu F, Xiao J, Xia QB, Li Z (2016) A novel bimetallic MIL-101(Cr, Mg) with high CO_2 adsorption capacity and CO_2/N-2 selectivity. Chem Eng Sci 147:109–117. doi:10.1016/j.ces.2016.03.035